Volume 61
Number 75
25 September 2025
Pages 14209–14460

ChemComm

Chemical Communications

rsc.li/chemcomm

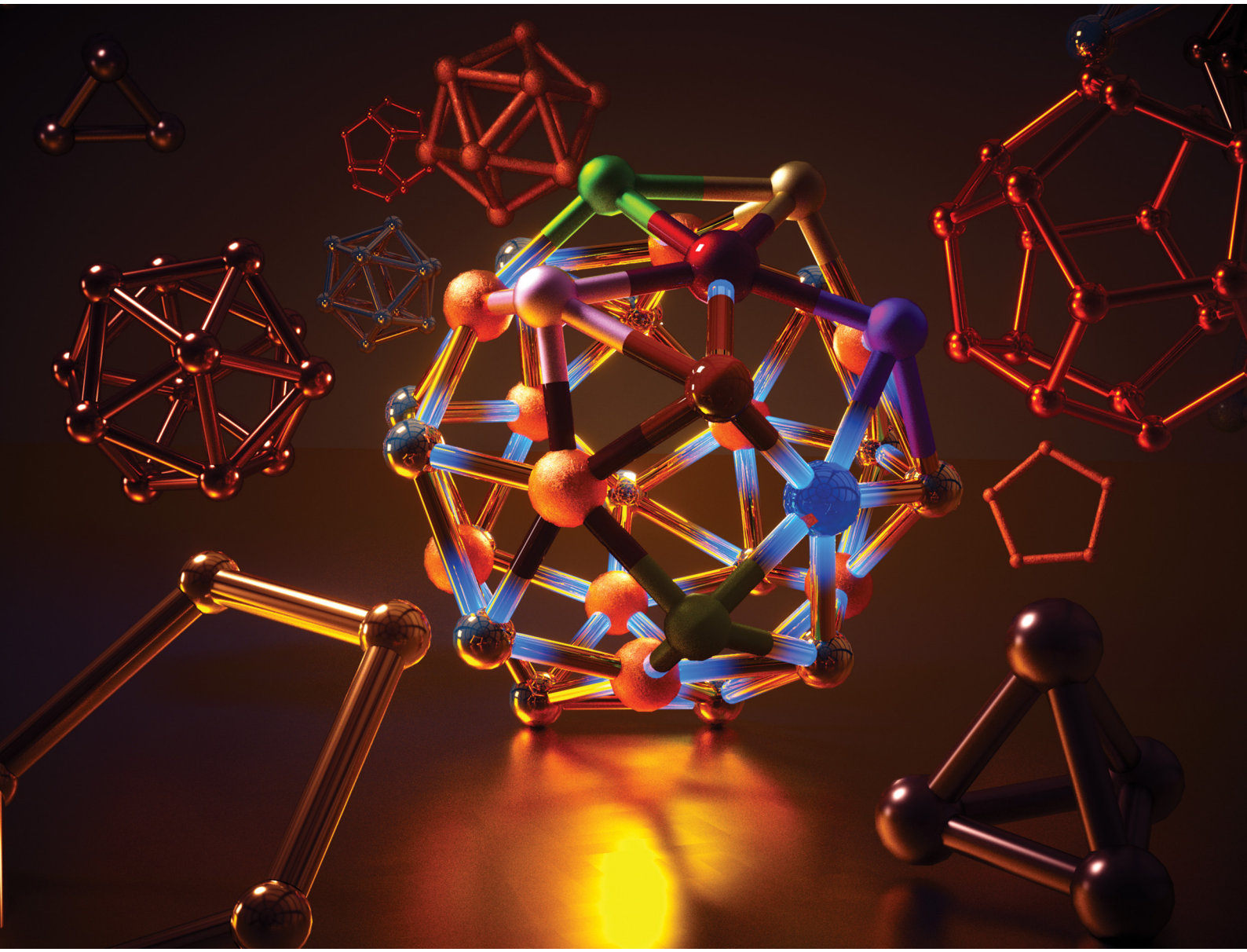

ISSN 1359-7345

ROYAL SOCIETY OF CHEMISTRY

FEATURE ARTICLE
Miquel Solà and Alvaro Muñoz-Castro
Aromaticity of all-metal clusters

ChemComm

FEATURE ARTICLE

View Article Online
View Journal | View Issue

Check for updates

Cite this: *Chem. Commun.*, 2025, **61**, 14280

Received 8th July 2025,
Accepted 6th August 2025

DOI: 10.1039/d5cc03842a

rsc.li/chemcomm

Aromaticity of all-metal clusters

Miquel Solà *[a] and Alvaro Muñoz-Castro *[b]

The first all-metal aromatic cluster, Al_4^{2-}, face-capped by an M^+ cation (M = Li, Na, Cu), was detected in 2001. Since then, several all-metal aromatic clusters have been extensively studied. Here, we review the most significant developments that have occurred mainly in our labs, including topics ranging from the difficulty of measuring aromaticity in metal clusters to the use of current techniques to investigate aromaticity in both small and large metal clusters.

Open Access Article. Published on 06 2025. Downloaded on 01.02.26 18:10:06.
This article is licensed under a Creative Commons Attribution-NonCommercial 3.0 Unported Licence.

1. Introduction

This year we celebrate the 200th anniversary of the discovery of benzene by Michael Faraday.[1] This molecule has become a reference molecule that is used when discussing aromaticity with experiments and theoretical methods. Comparison with benzene is reasonable for classical aromatic organic molecules such as polycyclic aromatic hydrocarbons (PAHs),[2] heteroaromatic organic compounds,[3,4] and nanographenes.[5] Such a comparison can also be performed when a C–H group in these compounds is substituted by an isolobal metal fragment leading to metallobenzenes, or heteroatom-containing analogues such as metallapyridines or metallapentalenes.[6,7] However, it is not applicable to all-metal clusters, which are aggregates of only metal atoms that exhibit aromatic characteristics. The aromaticity of all-metal aromatic compounds containing σ-, π-, δ- and ϕ-electron delocalization is far more complex than that of typical aromatic organic molecules, which possess π-electron delocalization only. Furthermore, these compounds have the ability to blend several forms of (anti)aromaticity, resulting in double or triple aromaticity—a phenomenon known as multifold (anti)aromaticity.[8–10] They can also display aromaticity in one (or several) component(s) (σ, π, δ or ϕ) and antiaromaticity in other(s), giving rise to the conflicting

[a] *Institut de Química Computacional i Catàlisi and Departament de Química, Universitat de Girona, 17003 Girona, Catalonia, Spain. E-mail: miquel.sola@udg.edu*
[b] *Facultad de Ingeniería, Universidad San Sebastián, Bellavista 7, Santiago 8420524, Chile. E-mail: alvaro.munozc@uss.cl*

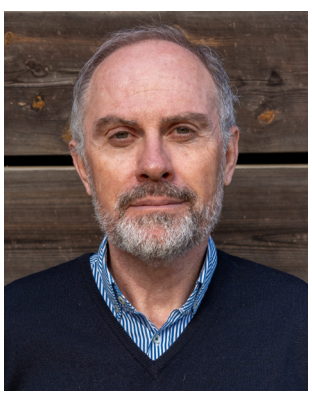

Miquel Solà

Miquel Solà obtained his PhD in 1991 with academic honours. In 1993, he moved to the University of Girona (UdG) as an assistant researcher. In 1994, he carried out postdoctoral research with Prof. Baerends and, in 1995, with Prof. Ziegler. He was appointed an assistant professor of the UdG in 1997 and a full professor in 2003. He was awarded with the ICREA Academia Prize three times (2009, 2014, and 2024). In 2013, he got the physical chemistry prize and, in 2025, the gold medal, both awarded by the Spanish Royal Society of Chemistry. His main interests are aromaticity, reaction mechanisms, and excited states.

Alvaro Muñoz-Castro

Alvaro Muñoz-Castro earned his PhD degree in molecular physical chemistry (2010) from Universidad Andres Bello, Chile, under the supervision of Ramiro Arratia-Pérez related to relativistic computational chemistry of inorganic species. Currently, he is a full-time professor at Universidad San Sebastián, Chile. His interests range from metallic clusters and superatoms, fullerenes, involving the understanding of the related bonding, optical, luminescent, magnetic and aromatic properties.

This journal is © The Royal Society of Chemistry 2025

Open Access Article. Published on 06 2025. Downloaded on 01.02.26 18:10:06.
This article is licensed under a Creative Commons Attribution-NonCommercial 3.0 Unported Licence.

aromaticity concept.[11,12] One can classify aromatic all-metal clusters based on the type of delocalized electrons (σ-, π-, δ-, ϕ-, and multifold) or take into account if they are relatively simple and planar or three-dimensional (3D). Here, we have preferred the latter classification.

In 2001, Li *et al.*[13] experimentally observed the Al_4^{2-} all-metal cluster in the form of the bimetallic clusters $LiAl_4^-$, $NaAl_4^-$, and $CuAl_4^-$, which in their most stable isomeric form contains a square-planar Al_4^{2-} dianion. These clusters were obtained using a laser vaporization technique and characterized using their experimental and theoretical photoelectron spectra. To rationalize chemical bonding in this cluster the authors looked at the chemical bonding in Al_4^{2-}, as they assumed that bonding between countercations (Li^+, Na^+, or Cu^+) and Al_4^{2-} is primarily ionic. For Al_4^{2-}, the total number of valence electrons is $3 \times 4 + 2 = 14$. As can be seen in Fig. 1, the four 3s atomic orbitals (AOs) of the Al atoms combine to give the σ_S system with four molecular orbitals (MOs): one bonding without nodes, two degenerate non-bonding with one node, and one antibonding with two nodes. These orbitals are completely filled with eight electrons. Same combinations of AOs take place with the set of four $3p_x$, $3p_y$, and $3p_z$ AOs generating the σ-radial (σ_r), σ-tangential (σ_t), and π systems, respectively, each of them occupied with two-electrons.[14] Therefore, with two electrons, the π-system follows the $4N + 2$ Hückel rule[15–18] and is considered aromatic. Although this is not the case for the σ-system with four electrons, the two pairs of delocalized σ-electrons belong to MOs that follow orthogonal radial (σ_R, orbital $2a_{1g}$) and tangential (σ_T, orbital $1b_{2g}$) directions, which makes them independent,[19] thus separately following the $4N + 2$ rule. Therefore, according to its electronic structure, Al_4^{2-} can be considered a three-fold aromatic system (σ_T, σ_R, and π). Thus, the Al_4^{2-} all-metal cluster is an example of multifold aromaticity, with the π-MOs resembling those of organic aromatic species, and the σ_r-MOs being similar to those found in σ-aromatic species such as H_3^+.[20] Calculations of multicenter indices (MCI), nucleus-independent chemical shifts (NICS), resonance energies, and ring currents support the aromaticity of Al_4^{2-}.[19,21–28] The discovery of all-metal aromaticity in Al_4^{2-} meant a complete revolution in the field, with many other all-metal aromatic clusters being discovered afterwards.[8,29–32]

Al_4^{2-} is the paradigmatic example of all-metal aromatic clusters. From the beginning, aromaticity has been associated with kinetically and thermodynamically stable compounds. By connecting the concept of aromaticity with stability, Hoffmann concluded that all-metal clusters such as Al_4^{2-} cannot be classified as aromatic because "aromatic molecules are 'bottleable'".[33] This is an interesting controversy. Only stable compounds can be aromatic? Several examples show that this is not the case. For instance, transition states of allowed pericyclic reactions are obviously nonbottleable species, but their aromaticity, which is widely accepted by the chemical community, is responsible, in part, for the relatively low barriers observed for this type of reaction.[34–40] As another example, certain excited states are aromatic and nonbottleable compounds, like those following Baird's rule.[41–43] This rule states that the lowest-lying triplet states of $4N$ π-electrons, such as the T_1 state of cyclooctatetraene, are aromatic. We do not think that the 'bottleable' criterion should be the one that prevails when classifying compounds as aromatic. In our opinion, following the definition by Chen *et al.*,[44] species in their ground or excited state showing cyclic π-electron delocalization that results in energy lowering and a tendency toward bond length equalization, particular magnetic behaviour, and characteristic spectroscopic features have to be classified as aromatic irrespective of whether they are 'bottleable'.

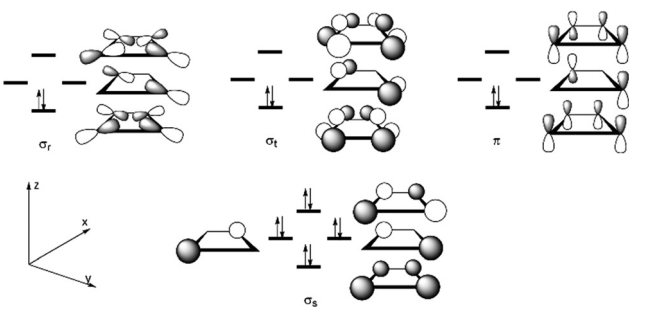

Fig. 1 Valence molecular orbitals of the Al_4^{2-} all-metal cluster. For the σ_T-, σ_R-, and π-MOs, only one of two degenerate MOs are displayed.

2. Quantifying aromaticity in all-metal clusters

From a theoretical perspective, assessing the aromaticity of all-metal aromatic compounds is necessary for a thorough investigation. The measurement of aromaticity in all-metal clusters is considerably more difficult than in classical organic compounds due to the presence of multifold and conflicting aromaticities and the lack of all-metal aromatic clusters that can act as inorganic reference systems (like benzene does in classical aromatic organic molecules). In fact, the majority of the methods for measuring aromaticity that are currently available were designed to assess the aromaticity of organic molecules using benzene or other aromatic organic compounds as a reference for their definitions. For example, the electronic-based descriptors like the bond order index of aromaticity (BOIA),[45] the aromatic fluctuation (FLU) index,[46,47] the aromaticity descriptor θ[48,49] or the structure-based harmonic oscillator model of aromaticity (HOMA)[50,51] are examples of this type of aromaticity indicator. Similarly, the absence of suitable reference systems[21,52] makes it challenging to compute energy-based markers like resonance energy (RE) or aromatic stabilization energy (ASE)[53] in all-metal clusters. In general, reference-system-based indices of aromaticity, without additional improvements, cannot be used directly to assess the aromaticity of all-metal clusters. Moreover, most of these reference-based methods do not allow for a study of the different types of aromaticity in species having multifold aromaticity, which represents another important disadvantage of these methods.

At this moment, there are three main groups of methods used to assess all-metal aromaticity. First, the magnetic-based indicators of aromaticity, which are based on the ring currents

Open Access Article. Published on 06 2025. Downloaded on 01.02.26 18:10:06.
This article is licensed under a Creative Commons Attribution-NonCommercial 3.0 Unported Licence.

that are generated when applying external magnetic fields to these compounds. Ring currents are not observable, but their effects are (in NMR spectra, for instance). The calculated ring currents are origin dependent. Several attempts have been performed to circumvent the gauge origin problem. The gauge-including magnetically induced currents (GIMIC)[54] and the continuous transformation of the origin of the current density (CTOCD)[55,56] methods are among the most widely used. To get additional information, one can depict these ring currents on the surface of the so-called anisotropy of the magnetically induced current density tensor (ACID).[57,58] Among the magnetic descriptors, one of the most widely used is the nucleus-independent chemical shift (NICS)[59] and its different variants such as NICS(0)$_{zz}$ and NICS(1)$_{zz}$ (the out-of-plane tensor component) or NICS(0)$_{\pi zz}$ and NICS(1)$_{\pi zz}$ (the π-orbital contribution),[44] as well as the NICS-scans analysis,[60–62] the NICS decomposition into canonical molecular orbital contributions (CMO-NICS),[63] and the different representations of the NICS values.[64–66] Among the NICS's many benefits, one finds its ease of use and accessibility and the clear separation that provides among aromatic (negative NICS values), non-aromatic (values close to zero), and antiaromatic systems (positive values), and the possibility of separation into σ-, π-, and δ-contributions.[60] It is worth noting that NICS and ring currents can be affected by the relativistic corrections when molecules that contain heavy elements are studied.[67] Moreover, the core electrons in heavy atoms can also generate NICS and ring currents that result in spurious aromaticity assessments.[68]

The second group corresponds to the methods that measure the cyclic delocalization of mobile electrons in closed circuits of two or three dimensions.[69] Cyclic delocalization is one of the basic and crucial characteristics of aromatic compounds. Since this electronic delocalization is not observable, there is no experimental property that permits its direct measurement. Because of this, there is no single, widely accepted computational method to measure it. Among the methods that provide measures of electronic delocalization[70] without making use of reference values, we can mention the multicentre delocalization index in a ring (I_{ring}),[71] which is a generalization of the delocalization index between two atoms,[72–74] the multicentre index (MCI),[45] an extension of the I_{ring} index, the electron localization function (ELF)[75] using the bifurcation values as a measure of aromaticity,[76,77] the localized orbital locator (LOL)[78–80] and its variant, LOL-π, which can be used to investigate π-electron delocalization,[81] and the electron density of delocalized bonds (EDDB)[82] that yields the number of electrons delocalized in a closed circuit as an indicator of aromaticity.[83] The advantages and drawbacks of all these methods have been discussed recently.[5] In particular, both the separation into α and β components and σ-, π-, and δ-contributions are possible.

The third group refers to the indicators of aromaticity that analyse the molecular structure. They are based on the fact that, in aromatic systems, there is usually an observed equalization of bond lengths. Then, one can use the degree of bond length alternation (BLA) as a quantitative measure of aromatic character in molecules.[84] This descriptor can be used only in rings made with a single metal, and, for this reason, is less used for the analysis of all-metal clusters than those of the two previous groups mentioned.

For the correct assessment of the aromaticity of all-metal clusters, we recommend the use of at least one indicator from each of the two former groups mentioned above. Moreover, together with the calculation of magnetic and electronic descriptors to verify electron delocalization, it is advisable to contextualize aromaticity in terms of the fulfilment of electron counting rules such as the $4N + 2$ Hückel's rule,[15–18] the $4N$ Baird's rule for the lowest-lying triplet excited states,[85] the $2(N + 1)^2$ Hirsch rule of spherical aromaticity,[86] *etc.* using either valence canonical MOs or, even better, MOs obtained from an adaptive natural density partitioning (AdNDP) analysis[87] or other localization schemes.

3. Simple all-metal aromatic species

Since the landmark realization of all-metal aromaticity in 2001, this field triggered considerable research studies driven by the extension of the concept of aromaticity offering unprecedented cases and unexpected structures setting solid bases for the current understanding of this transversal concept as summarized in earlier reviews and books.[8,31,88] Interestingly, their appearance is given even in biological relevant macromolecules as reported for the human copper chaperone Atox1.[89] When silver ions were mixed with copper chaperone Atox1, the resulting σ-aromatic $[Ag_4]^{2+}$ core was found to attenuate cancer cell proliferation.[90]

Regarding the smallest all-metal aromatic ring structure provided by M_3, some earlier examples are given by the *cyclo*-$[Mg_3]^{2-}$ cluster that can be stabilized with alkaline and alkaline-earth cations. The *cyclo*-$[Mg_3]^{2-}$ cluster has a triplet ground state with the singlet closed-shell state being almost degenerate.[91–93] The singlet closed-shell *cyclo*-$[Mg_3]^{2-}$ cluster is σ-aromatic and undergoes a dramatic aromaticity change to π-aromaticity when interacting with cations to form X_nMg_3 (n = 1, 2; X = Li^+, Na^+, K^+, Be^{2+}, Mg^{2+}, Ca^{2+}). Interestingly, the aromaticity of X_nMg_3 species can be tuned by modifying the X–Mg distance.[91] Another example of σ-aromaticity confirmed by NICS and MCI (Table 1) calculations is given by the Cu_3^+ species.[27,94] Multifold aromaticity in M_3 species is found in the d-orbital σ + π double aromaticity of valence isoelectronic Y_3^- and La_3^- clusters as confirmed by NICS, MCI, and resonance energies,[27,95] whereas Hf_3 shows three-fold σ-, π-, and δ-aromaticity according to both molecular orbital analysis and MCI results.[27] Even more interesting is the multifold aromaticity in the open-shell molecule $^5Ta_3^-$. The quintuplet $^5Ta_3^-$ is the lowest-lying spin state of Ta_3^-, and it exhibits three-fold σ-, π-, and δ-aromaticity based on MCI findings and molecular orbital analysis. Its σ- and π-aromaticities are of the open-shell Baird-type, whereas its δ-aromaticity is of the Hückel-type (a pair of closed-shell electrons).[27] On the other hand, the $[Ga_3(Mes_2C_6H_3)_3]^{2-}$ complex[96] displays an homometallic equilateral $[Ga_3]^+$ triangle with Ga–Ga distances of 2.441 Å. The metallic core exhibits a populated delocalized π-orbital fulfilling the Hückel rule, the overall structure being described as a metalloaromatic from related computational models.[97] Similarly, the isoelectronic and

 This journal is © The Royal Society of Chemistry 2025

Open Access Article. Published on 06 2025. Downloaded on 01.02.26 18:10:06.
This article is licensed under a Creative Commons Attribution-NonCommercial 3.0 Unported Licence.

Table 1 MCI, MCI_π, MCI_σ, and MCI_δ indices for Cu_3^+, Y_3^-, La_3^-, Hf_3, and $^5Ta_3^-$ at the B3LYP/X/Stuttgart + 2f (X = Cu, Y, and La) level of theory. All MCI values in electrons and bond distances in Å. All molecules are in their ground states. Values taken from ref. 27

	Cu_3^+	Y_3^-	La_3^-	Hf_3	$^5Ta_3^-$
	2.364	3.116	3.385	2.713	2.471
MCI	0.189	0.754	0.750	1.037	0.776
MCI_σ	0.188	0.458	0.454	0.445	0.362
MCI_π	0.001	0.296	0.296	0.296	0.178
MCI_δ	0.000	0.000	0.000	0.295	0.235
Aromaticity	σ	σ + π	σ + π	σ + π + δ	σ + π + δ

isostructural aluminium counterpart $[Al_3(Mes_2C_6H_3)_3]^{2-}$ reported by Power *et al.*[98] retains the aromatic characteristics in the $[Al_3]^+$ core. In addition, the boron-dinitrogen and boron-carbonyl cations generated in the gas phase, exhibit cyclic structures of the form $[B_3(NN)_3]^+$ and $[B_3(CO)_3]^+$ featuring a related $[B_3]^+$ core which similarly leads to two π-electrons, as the smallest π-aromatic kernel.[99] Such examples expose that for these species, it is plausible to shift from boron to gallium retaining similar aromatic characteristics and keeping the same aromatic motif decorated with different supporting ligands. A recent review on triangular all-metal aromatic cores has been provided.[100]

With respect to four membered metalloaromatic rings, Al_4^{2-} is the archetypal all-metal aromatic cluster. It has a total MCI value of 0.356 a.u. computed at the B3LYP/6-311+G(d) level of theory.[27] This value can be decomposed into a MCI_σ value of 0.169 a.u. and a MCI_π value of 0.187 a.u. indicating that the π-delocalization is slightly larger than the σ-delocalization, in agreement with NICS and ELF analyses.[76,101]

Among the different distortions that a benzene ring can suffer, the Kekulean or bond length alternation (BLA) distortion of the in-plane b_{2u} symmetry that changes the D_{6h} symmetry of benzene into a Kekulé-like D_{3h} symmetry structure is particularly interesting because it was found to be favoured by the π-electrons.[84,102–104] In the case of Al_4^{2-}, the π-electrons are also distortive, but their preference for a localized D_{2h} structure is weaker than in benzene. As for benzene, the σ-electrons enforce the regular D_{4h} equilibrium geometry with delocalized electron pairs.[105]

Ge_4^{2+} is an all-metal cluster that is valence isoelectronic with Al_4^{2-}. In fact, it has similar MCI (MCI = 0.386, MCI_σ = 0.187, MCI_π = 0.199 a.u.) and NICS values.[101] By performing successive substitution of Al atoms by more electronegative Ge atoms in Al_4^{2-}, we expect the following trend of aromaticity: $Al_4^{-2-} > Al_3Ge^- \geq Al_2Ge_2 \leq AlGe_3^+ < Ge_4^{2+}$. The same trend is expected for all the series of four-membered ring valence isoelectronic clusters $[X_nY_{4-n}]^{q\pm}$ (X, Y = Al, Ga, Si, and Ge; n = 0–4). This series was used to evaluate the reliability of NICS and MCI to provide the correct trends in all-metal and semimetal aromatic clusters.[101] It was found that MCI was superior to NICS in reproducing the expected trends in aromaticity. Among the different NICS-based indicators, the $NICS(0)_\pi$ was the one that performed the best.

The four-membered cyclic systems $M_2A_2^{2-}$ (M and A = B, Al, and Ga) are also valence isoelectronic with Al_4^{2-}. For the cases M ≠ A, the clusters can adopt *cis* (C_{2v}) and *trans* (D_{2h}) configurations. With the induced magnetic field and MCI calculations, the double σ + π aromatic character of these rings was confirmed.[106] In general, between C_{2v} and D_{2h} structures, the most aromatic ring is also the most stable, except for $Al_2B_2^{2-}$ and $Ga_2B_2^{2-}$, for which the strong B–B bond present in their C_{2v} structures has an important stabilization role. The $M_2A_2^{2+}$ (M and A = C, Si, and Ge) species are also valence isoelectronic with the $M_2A_2^{2-}$ (M and A = B, Al, and Ga) clusters and they also show σ- and π-aromaticity. However, contrary to what was found for group 13 $M_2A_2^{2-}$ clusters, the linear isomer of group 14 $M_2A_2^{2+}$ clusters is the most stable for two of the clusters ($C_2Si_2^{2+}$ and $C_2Ge_2^{2+}$) and it is isoenergetic with the cyclic D_{4h} isomer in the case of C_4^{2+} (see Fig. 2).[107]

The first all-metal with π-antiaromaticity was $Li_3Al_4^-$, which contains a planar and rectangular Al_4^{4-} unit.[11] Interestingly, the singlet (S_0) and the lowest-lying triplet (T_1) states of Al_4^{4-} are almost degenerate, with the singlet state being more stable by just 1.6 kcal mol^{-1} at the (U)B3LYP/6-311+G(d) level of theory.[108] In S_0, the two electrons added to Al_4^{2-} to get Al_4^{4-} goes to one of the degenerate π-MOs of Al_4^{2-} (Fig. 1). With these two electrons, the π-system with four electrons becomes antiaromatic, whereas the σ-system keeps its aromaticity. Therefore, Al_4^{4-} in its closed-shell singlet state has conflicting aromaticity since it has an aromatic σ-component and an antiaromatic π-component. In the

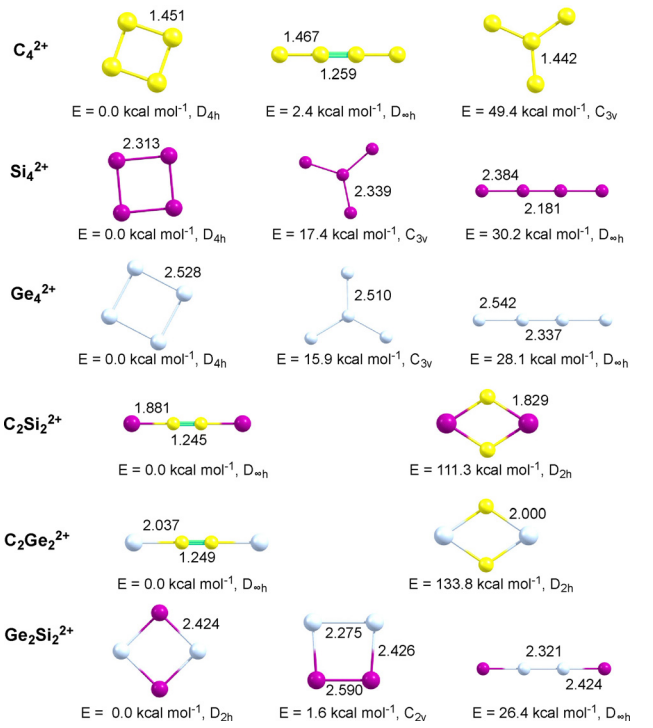

Fig. 2 Optimized geometries of most stable $M_2A_2^{2+}$ clusters of group 14 computed using the PBE/TZ2P method. Bond lengths in Å and CCSD(T)/6-311G*//PBE/TZ2P relative energies in kcal mol^{-1}. Reprinted with permission from ref. 107. Copyright Royal Society of Chemistry, 2016.

Open Access Article. Published on 06 2025. Downloaded on 01.02.26 18:10:06. This article is licensed under a Creative Commons Attribution-NonCommercial 3.0 Unported Licence.

T_1 state, the two unpaired electrons of Al_4^{4-} occupy σ_r degenerate MOs (Fig. 1) in a D_{4h} symmetric structure. In this state, the cluster is Baird σ_r-aromatic and Hückel σ_t- and π-aromatic. The extra stabilization of the T_1 state comes from this Baird aromaticity.[108] A similar situation is found for the T_1 states of Be_2B_6 and $Be_2B_7^+$, which are Baird σ-aromatic and Hückel π-aromatic. However, in these molecules, the lowest-lying triplet is clearly the ground state.[108] In contrast, $Be_2@Be_6H_6$, which has also a triplet ground state, has Hückel σ-aromaticity and Baird π-aromaticity.[109]

Finally, a σ-aromatic neutral rhombic Al_2Pd_2 cluster has been recently reported. Its aromaticity has been confirmed by AdNDP, NICS, ACID, ELF, EDDB, GIMIC and MO analysis. The system presents a 4c-2e σ-bond that provides the σ-aromaticity.[110]

4. All-metal clusters with spherical aromaticity

Spherical all-metal clusters expose the delicate and challenging balance between both electronic shells and structural features, as a result of the quantum confinement of electrons,[111–114] which are highly desired as building blocks in molecularly conceived materials. Since the discovery of buckminsterfullerene (C_{60}) and related species,[115,116] an increasing interest has been focused on the use of stable three-dimensional cages with particular properties, leading to them being widely explored, where fullerenes have been proved to be highly versatile building blocks in nanotechnology.[117,118] The unique spherical structure of fullerenes, along with the surface full of π-electrons, possesses many fascinating properties and generates a wide range of applications in biology, medicine, and electronics.[119–121] Moreover, the internal cavity of fullerenes provides a suitable region for hosting atoms and molecules, giving rise to a whole new class of endohedral clusters, named endofullerenes.[122–124] Despite the structural stability, the 60 π-electrons in the curved C_{60} initially ascribed as a prototypical spherical aromatic molecule,[115,125–127] shifted to a more appropriate non-aromatic character[128] owing to the local aromatic and antiaromatic character displayed by hexagons and pentagons, respectively. Moreover, it is endowed with spherical aromatic character after reduction, as highlighted for the hexaanion C_{60}^{6-} formed in alkali-metal fullerene phases.[129–132]

The rapid progress in fullerene-related clusters and the extensive applications for fullerene-based materials encourage the promising exploration of analogous hollow spheres composed of main-group or transition metal elements known as inorganic fullerenes. One of the earliest proposals was provided by Johansson and coworkers, who, following the Hirsch rule of spherical aromaticity $2(N+1)^2$ with $N=3$, were able to predict and locate the existence of an all-metal aromatic fullerene counterpart given by Au_{32},[133] featuring a sizable HOMO–LUMO gap in a symmetrical icosahedral structure. The reported central NICS value inside the cage is -100 ppm,[133] largely increased in comparison to that for C_{60} at the same level of theory (-2 ppm), supporting the spherical aromatic characteristic of this golden fullerene proposal, where the icosahedral structure is favoured as denoted in earlier works and in the characterization from laser vaporization of a gold foil by Wang.[134,135] Using the same approach, Pyykkö and coworkers[136] were able to account for larger related species, highlighting the chiral structure of the Au_{72} golden fullerene satisfying the Hirsch rule $2(N+1)^2$ with $N=5$, featuring 72-cluster electrons, giving rise to a spherical aromatic hollow cluster with a central NICS value of -111 ppm. For Au_{50}, satisfying the $2(N+1)^2$ rule with $N=4$, also depicts a central shielding NICS value of -88.5 ppm, where in contrast, the also spherical structure of Au_{42} shows antiaromatic character as seen from the NICS value of 125 ppm.

One of the guiding principles for identifying systems with spherical aromaticity is the $2(N+1)^2$ Hirsch rule. An alternative to this rule is to look for whether the system under consideration (usually a molecular cluster) has, for the valence electrons, an electronic structure with a closed-shell configuration on the basis of the jellium model.[137–139] The energy levels of the valence electrons for such a model are $1S^21P^61D^{10}2S^21F^{14}2P^61G^{18}2D^{10}3S^2\ldots$, where S, P, D, F, and G letters denote the angular momentum and numbers 1, 2, and 3 indicate the radial nodes. The abundance of alkali metals, alkaline earth metals, and gold clusters bearing 2, 8, 18, 20, 34, 40, 58, 68, 70, 92,... electrons found in experimental mass spectra are justified by taking into account the fact that these numbers of electrons reach closed-shell electronic structures in the jellium model.[140,141] An extension of the Baird's rule for the jellium model was also proposed in 2019.[142] Clusters whose last energy level of valence electrons is half-filled with same-spin electrons in the jellium electronic structure are aromatic and present extra stability compared to those that do not have this electronic structure. This situation is reached for the magic numbers of valence electrons of 1 ($S=1/2$), 5 ($S=3/2$), 13 ($S=5/2$), 19 ($S=1/2$), 27 ($S=7/2$), 37 ($S=3/2$), 49 ($S=9/2$),... Na_{19} with $S=1/2$ or Be_{13}^- clusters with $S=7/2$ are examples of this open-shell jellium stability. Interestingly, some metal clusters follow more than a single rule. For instance, Li_6^+ ($S=3/2$) follows both the $2N^2+2N+1$ with $S=N+1/2$ ($N=1$) for open-shell spherical aromaticity and the open-shell jellium rules[143] (*vide infra*).

The quest for all-metal fullerene counterparts is promising, encouraging their synthesis from wet methods to further explore their novel chemistries. In this respect, it is worth mentioning the crystallization of the $[K@Au_{12}Sb_{20}]^{5-}$ anion obtained after reaction of the Zintl phase K_8SnSb_4 with $Au(PPh_3)Me$ in the ethylenediamine solution by Sun and coworkers.[144] The resulting structure reveals a highly symmetrical cluster featuring a dodecahedral Sb_{20} cage with each five-membered face decorated with an Au atom, sustaining a backbone composed of Au–Sb bonds, where a K^+ cation is allocated inside the cluster. Interestingly, the AdNDP analysis reveals twenty 1c-2e lone pairs at each Sb atom, thirty 4c-2e σ-bonds lying at the cluster surface, in addition to the sixty Au-5d lone pairs. The remaining 18 electrons inside the cage (cluster electrons) give rise to nine occupied orbitals featuring a superatomic shell structure given by the $1S^21P^61D^{10}$ configuration, which fulfils both the jellium closed-shell structure and the $2(N+1)^2$ rule with $N=2$, satisfying the spherical aromatic requirements contributing to the overall stabilization of the cluster, as pointed out from the electronic criteria of aromaticity. To further evaluate the spherical aromatic in the $[K@Au_{12}Sb_{20}]^{5-}$

 This journal is © The Royal Society of Chemistry 2025

Open Access Article. Published on 06 2025. Downloaded on 01.02.26 18:10:06.
This article is licensed under a Creative Commons Attribution-NonCommercial 3.0 Unported Licence.

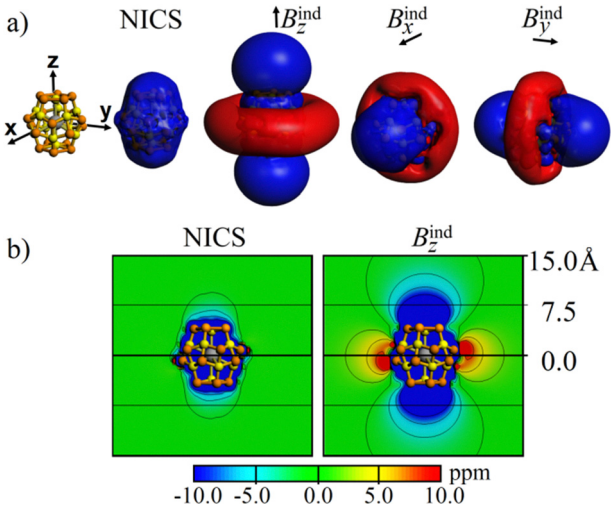

Fig. 3 Magnetic response properties of $[K@Au_{12}Sb_{20}]^{5-}$ from NICS isosurfaces and under specific orientations of the external field accounting for B_z^{ind}, B_x^{ind}, and B_y^{ind} isosurfaces, denoting both isosurface (a) and contour plot (b) representations. Isosurfaces are set at ±3.0 ppm, blue – shielding; red – deshielding.

anion, the NICS isosurface was calculated (Fig. 3), leading to a spherical-like shielding surface ascribed to the cluster backbone, which is common in spherical aromatic fullerenes,[145] resulting in a common characteristic in both organic and all-metal spherical aromatic fullerenes. In addition, under specific orientations of the external field, long-range shielding cone characteristics are enabled as obtained from representative orientations aligned with the *z*-, *x*-, and *y*-axis, which shows values of −20.0 ppm at 7.5 Å from the centre of the structure, and of −2.6 ppm at 15.0 Å. Such shielding cone characteristics enabled from any orientation of the external field are inherent to spherical aromatic species,[146] as an exclusive aspect of spherical aromatic species which is not obtained in planar aromatic species such as benzene.[145,147,148]

Thus, finding persistent structures leading to suitable building blocks may be guided by both electronic and magnetic criteria of aromaticity. The resulting chemical and physical characteristics of the designed clusters can be explored further. For instance, Mondal and Chattaraj denote aromatic clusters as interesting species that can be used in hydrogen storage applications.[149]

5. Octahedral aromaticity in all-metal clusters

Systems described as spherical aromatics have either a closed-shell structure (*e.g.* Au_{32}) or a half-filled shell with same spin structure (*e.g.* Be_{13}^{-} with $S = 7/2$). This recipe was applied in the quest of all-metal clusters with octahedral (O_h) aromaticity. To this end, we analysed all octahedral clusters of the type X_6^q with X = Li–C and Be–Si and $q = -2$ to +4 in $^{2S+1}A_{1g}$ electronic states (S = 0 to 3).[150] A typical octahedral cluster with a closed-shell electronic structure has the MO energy levels shown in Fig. 4. This is the situation of, for instance, Si_6^{2-}.[151] With this MO structure, the series 2, 8, 12, 14, 20, 26, 32, and so on could be suggested as the magic numbers that result in closed-shell octahedral aromatic species based on these MOs. The magic numbers for open-shell clusters could be 1, 5, 10, 13, 17, 23, and 29. Unfortunately, because the energy order of the MOs in Fig. 4 varies according to the X atoms, as well as the multiplicity and charge of the O_h $^{2S+1}A_{1g}$ X_6^q clusters, these series of magic numbers cannot be generalized. For the clusters of the second period (X = Li, Be, and B), the $2a_{1g}$ and $1t_{2g}$ MOs invariably become more stable than the $1e_g$ ones. Furthermore, the $2a_{1g}$ are more stable than the $1t_{2g}$ in some clusters, and *vice versa* in others. In general, the ordering of the various orbitals varies from cluster to cluster, and the energy difference between $1e_g$, the radial $2a_{1g}$, and the tangential $1t_{2g}$ is minor. This leads to the conclusion that it is not possible to derive a general rule for octahedral aromaticity similar to those of spherical aromaticity.

Calculations showed that, in general, O_h systems with closed-shells or open-shells half-filled with same spin electron systems have large multicentre indices and negative NICS values, as expected for aromatic compounds. These results confirm the existence of octahedral aromaticity in all-metal clusters like those found previously in Be_6 in its quintet state[152] and the singlet Au_6^{2-} and Al_6^{2-} clusters.[114,153]

Interestingly, despite B and Al belonging to the same group 13 elements, Al_6^{2-} favours the O_h structure, whereas the B_6^{2-} cluster prefers the planar D_{2h} geometry. Energy decomposition analysis based on the turn-upside-down approach concluded that is the orbital interaction term, which combined with the electrostatic component do (Al_6^{2-}) or do not (B_6^{2-}) compensate the higher Pauli repulsion of the O_h form.[154,155] These findings are consistent with the tendency for more localized bonding in

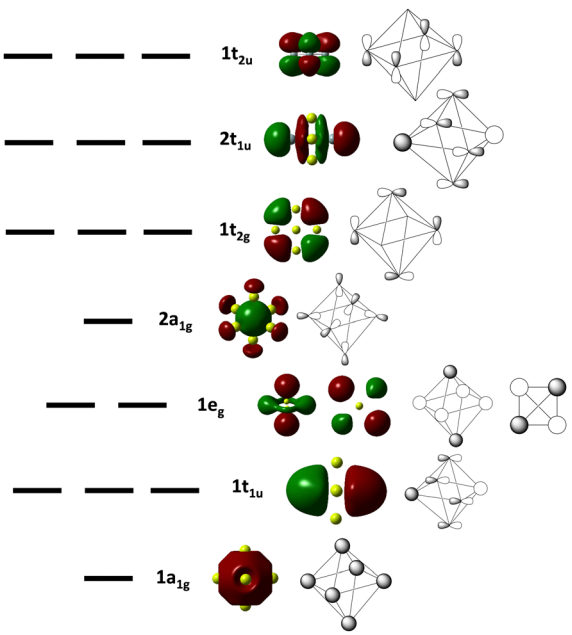

Fig. 4 Schematic representation of the molecular orbitals in an octahedral cluster. Reprinted with permission from ref. 150. Copyright Royal Society of Chemistry, 2016.

Open Access Article. Published on 06 2025. Downloaded on 01.02.26 18:10:06.
This article is licensed under a Creative Commons Attribution-NonCommercial 3.0 Unported Licence.

B metal clusters and a dominant delocalization force in Al clusters. Similar to B_6^{2-}, mixed clusters $Al_xB_y^{2-}$ ($x + y = 6$) with $y > 2$ favour the planar structure.

A special example of octahedral aromaticity is given by $^4A_{1g}$ Li_6^+ and $^5A_{1g}$ Be_6 all-metal clusters.[143] These two species have a large number of non-nuclear attractors (NNAs),[156] with all or almost all valence electrons located in these NNAs. The chemical bonding arrangement of these systems is reminiscent of solid metals, where metal cations are encircled by a ''sea'' of delocalized valence electrons. This is because these NNAs exhibit extremely delocalized electron densities. These new types of compounds were named metal cluster electrides,[143] to differentiate them from the molecular electrides,[157] which have an electron (or a high portion of an electron) that cannot be assigned to any nucleus of the molecule and is located in a NNA.

6. Zintl-ion clusters

Zintl-ion chemistry[158–161] extends the rich structural and composition diversity of all-metal clusters, constantly challenging our notion of chemical bonding[159–167] and related properties, featuring electron-deficient cages and multicentre bonding elements.[167–169] The relation between electron counts and structural characteristics has been classically understood in terms of the Wade–Mingos rules,[170–172] which correlate the number of vertices (n) and cluster electrons (ce) in such species. Deltahedral clusters displaying a −2 charge form electron-precise species fulfilling the Wade's $2n + 2$ skeleton electron count for *closo*-species, and $2n$ lone pairs of electrons, according to the vertex number, n, as denoted for representative Zintl-ion bare clusters.[168,173–177]

In 2000, using the proposal of the $2(N + 1)^2$ Hirsch rule,[86,178] the spherical aromaticity of the representative E_4^{4-} and $E_9^{2-/4-}$ (E = Si, Ge, Sn, Pb) clusters,[179] was rationalized in terms of separating between $2(N + 1)^2$ σ- and $2(N + 1)^2$ π-electron kernels, involving both tangential and radial orbitals, respectively. In this sense, the notion of spherical aromaticity in Zintl ions favours the recognition of such a property in a variety of three-dimensional structures of different shapes, composition, and bonding characteristics,[167] favouring the extension of this concept to all-metal three-dimensional clusters.

For highly symmetric clusters given by the icosahedral stannaspherene and plumbaspherene ($[Sn_{12}]^{2-}$ and $[Pb_{12}]^{2-}$) cages,[180–182] their electron count meets both Wade's $2n + 2$ and the Hirsch $2(N + 1)^2$ ($N = 4$) electron counts, resulting in representative spherical aromatic clusters as probed by the magnetic criteria of aromaticity, where the role of relativistic corrections[183] and core electrons has been discussed.[68] The aromatic characteristics of the hollow icosahedral cages are retained for metal encapsulated counterparts given by $[M@Pb_{12}]^q$ (M = Co, Rh, Ir, Au; $q = -3$, and, M = Ni, Pd, Pt; $q = -2$),[175,184] also noted as intermetalloid clusters,[185] highlighting the formation of a long-ranged shielding cone under the application of an orientation fixed external magnetic field. In addition, a good agreement is achieved in the calculation of ^{207}Pb-NMR parameters, which further supports the quantities obtained for the magnetic criteria of aromaticity.[175] Moreover, for the proposed $[Ca^{2+}@Pb_{12}^{2-}]$ cluster,[186] a long-range shielding region is enabled for particular orientations of the external field, indicating that this behavior is inherent to the $[Pb_{12}]^{2-}$ cage. Similar features have been described for $[E_9]^{4-}$ species, as given for $[Ge_9]^{4-}$.[187]

The chemical bonding analysis provided by the adaptive natural density partitioning (AdNDP) algorithm,[87] offers a realization of the bonding elements acting in the overall cluster, which has been employed to evaluate the $[Pb_4]^{4-}$, $[Pb_5]^{2-}$, $[Pb_9]^{4-}$, $[Pb_{10}]^{2-}$, and $[Pb_{12}]^{2-}$ clusters.[188] For $[Pb_4]^{4-}$, the 20 ce are distributed in four 1c-2e lone-pairs and six 2c-2e σ-bonds; similarly, the 40 ce in $[Pb_9]^{4-}$ shows nine 1c-2e lone-pairs and eleven multicentre σ-bonds, showing 3× 4c-2e, 3× 5c-2e, and 5× 8c-2e bonding elements in its C_{4v} geometry and 2× 3c-2e and 9× 5c-2e in the D_{3h} structure. In addition, for $[Pb_{12}]^{2-}$ an alternative bonding pattern is obtained using the AdNDP method, in comparison to canonical molecular orbitals,[181] revealing a set of twelve 1c-2e lone-pairs, six 5c-2e σ-bonds, and seven 10c-2e σ-bonds.[188] In addition, a more delocalized view of AdNDP for the $[Pb_{12}]^{2-}$ cluster[186] has been provided for the related $[Ca^{2+}@Pb_{12}^{2-}]$ cluster, given by twelve 1c-2e lone-pairs, nine 13c-2e and four 12c-2e delocalized bonds. From both magnetic and electronic descriptors, the spherical aromaticity in such species is supported, providing a qualitative proof of these characteristics.

Besides spherical aromatics, Zintl ions or intermetalloids also exhibit planar aromatic characteristics,[189–191] among other types of aromaticities,[192] unravelling examples of the increased versatility in the chemistry of these clusters. The characterization of $[Sn_5]^{6-}$ and $[Pb_5]^{6-}$ as five-membered planar rings has been provided by Sevov,[193,194] showing that such species resemble the π-orbitals from the 6π aromatic cyclopentadienyl anion, $C_5H_5^-$, ascribing such species to heavy-metal aromatic rings. The overall 26 ce are distributed in five 1c-2e lone-pairs, five 2c-2e σ-bonds, and in a set of three 5c-2e delocalized π-bonds, which meets the $4N + 2$ Hückel rule. It is noteworthy that aromatic 2π electron Ga_5 rings in $[Ga_5(CH(SiMe_3)_2)_5]^{2-}$ have been characterized,[195] which exhibit a single 5c-2e delocalized π-bonding element, enabling electronic delocalization as probed by magnetic descriptors from magnetically induced ring currents and NICS values. Thus, two isostructural rings are able to sustain aromatic characteristics despite the different π-electron count fulfilling the Hückel rule.

Recently, in two separate reports, the characterization of five-membered rings Sb_5^- and Bi_5^- is provided,[189,190] highlighting the presence of induced ring currents from magnetic descriptors, with diatropic currents with a strength of 14.4 nA T^{-1}, which is comparable to the calculated for the cyclopentadienyl anion (12.8 nA T^{-1}). In addition, the AdNDP analysis exhibits five 1c-2e lone-pairs, five 2c-2e σ-bonds, and a set of six π-electrons, thus, supporting the planar aromatic characteristics of both magnetic and electronic descriptors. In addition, the role of relativistic effects, particularly the spin–orbit coupling in the $[M_5]^-$ series (M = N, P, As, Sb, Bi, Mc) has been discussed in the literature,[196] denoting a very relevant role in the heavier members, exposing

 This journal is © The Royal Society of Chemistry 2025

Open Access Article. Published on 06 2025. Downloaded on 01.02.26 18:10:06.
This article is licensed under a Creative Commons Attribution-NonCommercial 3.0 Unported Licence.

the requirement of taking into account such effects to achieve a proper magnetic evaluation of these systems. Thus, extending the aromaticity concept to cases where relativistic effects are crucial favours an equal footing treatment and evaluation of aromatic species across the periodic table. Moreover, it is shown that $[Sb_5]^-$ and $[Bi_5]^-$ rings enable the formation of M–M bonds from coordinating metal atoms located on the faces of such rings,[189] in analogy to the recent characterization of the B_9 cluster.[197] M_5 aromatic rings are recursive motifs, as has been found in several species mimicking the coordinating chemistry of cyclopentadienyl anions, which has been collected and discussed in a previous review from Boldyrev and Sun.[167]

In addition to 2π and 6π aromatic rings, solid phases of the stoichiometry of $Ba_4Li_2Si_6$ and $Ba_4Li_2Ge_6$ reveal six-membered cyclic Zintl-ions motifs of the $[Si_6]^{10-}$ and $[Ge_6]^{10-}$ forms, respectively, highlighting the formation of aromatic 10π Hückel aromatic rings.[198]

Smaller aromatic ring members have also been isolated, as for example, the σ-aromatic $[Bi_4]^{4+}$ ring sustaining an induced ring current strength of 9.1 nA T^{-1}, lower in comparison to the seminal $[Al_4]^{4-}$ cluster (14.8 nA T^{-1}).[199] And aromatic three-membered rings have been characterized in $[As_3Nb(As_3Sn_3)]^{3-}$ and $[Sb_3Au_3Sb_3]^{3-}$, among others.[167] These examples expose both structural and chemical bonding versatility of Zintl-ions, enabling them to achieve an aromatic behaviour favouring a stable situation (*vide infra*). Given this rich diversity, the choice of an appropriate aromaticity descriptor is challenging, where the recommendation to involve at least both magnetic and electronic descriptors is suggested to be particularly useful in providing reliable results from different points of view, owing to the multidimensional character of this concept.[200]

Other outstanding species have been characterized involving several structural layers, which serves as an extension of the spherical aromaticity in endohedral $M@E_{12}$ species. The intermetalloid cluster coined as "a bronze matryoska" characterized by Fässler, involves three concentric structural layers,[201] featuring an inner Sn atom, encapsulated into a Cu_{12} icosahedron coated by a Sn_{20} dodecahedron with the formula $[Sn@Cu_{12}@Sn_{20}]^{12-}$. This prototypical spherical structure is based on the icosahedron–dodecahedron duality according to the number of vertices and faces, where the icosahedron has 20 faces and 12 vertices, and the dodecahedron has 12 faces and 20 vertices. Besides its aesthetically pleasing structure, this outstanding architecture serves as a prototypical case study to unravel the aromatic characteristics in multilayer clusters. The AdNDP analysis of $[Sn@Cu_{12}@Sn_{20}]^{12-}$ reveals thirty 4c-2e σ-bonds as bonding elements connecting the two atoms from the outer Sn_{20} cage (Fig. 5) to two adjunct Cu atoms from the internal Cu_{12} icosahedral cage.[202] Interestingly, the remaining 8 electrons are delocalized over the overall $Sn@Cu_{12}$ cage, resulting in a set of four 13c-2e bonds which satisfy the Hirsch rule of spherical aromaticity,[179] suggesting that both inner structural layers feature electronic delocalization giving rise to spherical aromatic properties.

Furthermore, the plausible formation of a spherical aromatic cluster for $[Sn@Cu_{12}@Sn_{20}]^{12-}$ has been evaluated *via* the magnetic criteria of aromaticity, which shows a shielding

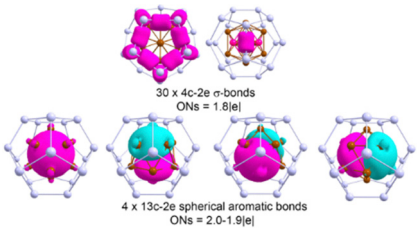

Fig. 5 Bonding pattern of $[Sn@Cu_{12}@Sn_{20}]^{12-}$. Copper atoms are brown. Reproduced with permission from ref. 202. Copyright Wiley, 2020.

region ascribed to the structural backbone, as noted from the isotropic term (B_{iso}^{ind}), also noted as the NICS isosurface (Fig. 6). From specific orientations of the external field, a long-ranged shielding cone characteristic is enabled, which extends to 11.5 Å from the centre of the structure with shielding values of −3.0 ppm and to 16.0 Å with values of −1.0 ppm. Such observations further support the spherical aromaticity of this multi-layered cluster, serving as a prototypical case for further identification of similar aromatic clusters. Interestingly, such observation is similar to that given for fullerenes and endohedral metallofullerenes,[203–206] suggesting the equal footing treatment of aromaticity in these structures based on the magnetic criteria of aromaticity.

Now, we turn our attention to structures seen as the aggregation of individual cluster building blocks. In this issue, the $[Pd_2@E_{18}]^{4-}$ clusters (E = Ge, Sn) has been rationalized as the fusion of parent spherical aromatic $[Pd@E_{12}]^{2-}$ building units,[207,208] resulting in an interesting intercluster bonding pattern, leading to an overall bond order of 2.70 and 2.31 for $[Pd_2@Ge_{18}]^{4-}$ and $[Pd_2@Sn_{18}]^{4-}$, respectively.[209] Moreover, to evaluate the plausible aromatic behaviour in this structure involving two fused clusters, the characteristics of the induced magnetic field have been obtained, showing a related shielding surface contained within the oblate cage from the NICS isosurface (Fig. 7). When compared to the $[Pd@E_{12}]^{2-}$ parent cluster, the NICS isosurface in $[Pd_2@E_{18}]^{4-}$ is centred on both sides, denoting aggregation of two building units. Under specific orientations of the external field the shielding cone characteristics in the parent cluster are enabled, which are enhanced after formation of the $[Pd_2@E_{18}]^{4-}$ clusters, denoting the spherical aromatic characteristics of the overall structure as the fusion of two spherical aromatic cluster units.

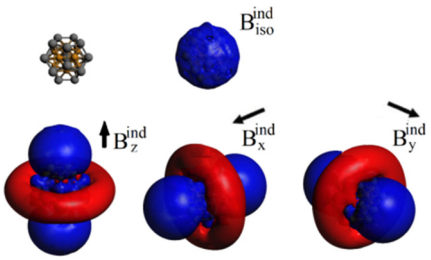

Fig. 6 Magnetic response properties of $[Sn@Cu_{12}@Sn_{20}]^{12-}$, denoting the isotropic (averaged) term (B_{iso}^{ind}), also noted as NICS isosurfaces, and under specific orientations of the external field (B_z^{ind}, B_x^{ind}, and B_y^{ind}). Isosurfaces set to ±3 ppm, blue – shielding; red – deshielding. Reproduced with permission from ref. 202. Copyright Wiley, 2020.

Open Access Article. Published on 06 2025. Downloaded on 01.02.26 18:10:06.
This article is licensed under a Creative Commons Attribution-NonCommercial 3.0 Unported Licence.

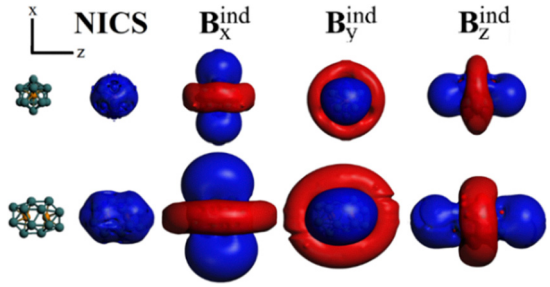

Fig. 7 Magnetic response properties of $[Pd_2@Sn_{18}]^{4-}$, denoting the NICS isosurfaces, and from specific orientations of the external field (B_z^{ind}, B_x^{ind}, and B_y^{ind}). Isosurfaces set to ±3 ppm, blue – shielding; red – deshielding. Reprinted with permission from ref. 209. Copyright Royal Society of Chemistry, 2024.

Lastly, the aggregation of three cluster units in a cyclic array is accounted for through the recent $[Co_3@Ge_6Sn_{18}]^{5-}$ structure,[210] which can be viewed as the aggregation of three $[Co@Ge_3Sn_6]^{4-}$ building units. This cluster features 32 electrons, retaining the bonding per each fused cluster unit, giving rise to three superatomic units with a filled $1S^21P^61D^{10}1F^{14}$ electronic closed-shell. In addition, two electrons are delocalized in the overall cluster structure in a 27c-2e σ-bonding element, which fills a bonding combination of three 2S shells centred at each building unit, sustaining a bonding 2S + 2S + 2S combination leading to cyclic cluster-of-cluster bonding characteristics. Interestingly, this 27c-2e bonding element is analogous to the 3c-2e bonding in H_3^+ and Li_3^+, suggesting the extension of aromatic properties from these small triatomic rings to a large cluster-based aggregate. Interestingly, from the global electron density of delocalized bonds,[211–213] it is pointed out that the electronic delocalization is of global character, involves the entire cluster, which is also supported by calculating the magnetically induced currents from the GIMIC suite[54,214] and analysis of the induced magnetic field (Fig. 8). From the NICS isosurface, the continuous shielding region is centred at each cluster building unit, resulting in three adjacent shielding regions. Under specific orientations of the external field, the overall $[Co_3@Ge_6Sn_{18}]^{5-}$ cluster structure enables shielding cone characteristics when the external field is oriented through the

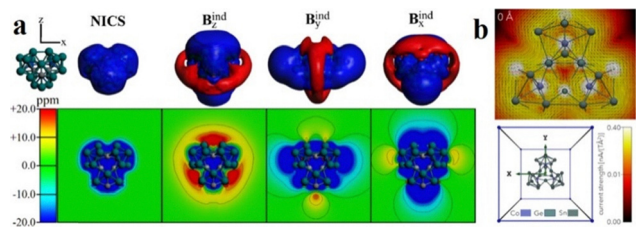

Fig. 8 (a) Isosurface and contour plot representation of the magnetic response properties for $[Co_3@Ge_6Sn_{18}]^{5-}$, denoting the NICS (isotropic/averaged) term, and from different orientations of the external field (B_x^{ind}, B_y^{ind}, and B_z^{ind}). Isosurfaces set to ±8 ppm, blue: shielding; red: deshielding. (b) Current density of the $[Co_3@Ge_6Sn_{18}]^{5-}$ cluster at the central plane located at 0 Å, containing the $[Co_3Ge_3]$ ring. The calculations were performed at the PBE0/def2-TZVP level of theory, without including solvent effects. Reprinted with permission from ref. 210. Copyright 2025 American Chemical Society.

z-axis (B_z^{ind}), in line with the appearance of the delocalized 27c-2e bonding element fulfilling the Hückel rule for aromaticity. Thus, this structure is ascribed as the first σ-bonded cluster trimer unravelling a σ-aromatic character, reported to date. Moreover, under parallel orientations (B_x^{ind} and B_y^{ind}), a similar long-range shielding cone is obtained originating at each building unit, denoting that besides the electronic delocalization in the overall $[Co_3@Ge_6Sn_{18}]^{5-}$ cluster structure, the inherent spherical aromatic characteristics of the constituent building units are retained.

Note that from the results obtained for the $[Pd_2@Sn_{18}]^{4-}$ dimer and $[Co_3@Ge_6Sn_{18}]^{5-}$ trimer, under different orientations of the external field, long-range shielding regions are enabled which are complemented with a perpendicular deshielding region, which nicely resemble the classical shielding cone properties from planar aromatics,[147,215,216] but enabled from any orientation in spherical aromatic species owing to its three-dimensional character.

7. Conclusions

The exploration of aromaticity in all-metal clusters has deeply reshaped our understanding of this fundamental chemical concept. Unlike the straightforward rules governing classical organic molecules, all-metal clusters introduce remarkable complexity, often displaying multifold (anti)aromaticity in the σ-, π-, δ- or ϕ-electron delocalization paths or conflicting aromaticity among several of these components. To navigate this intricate landscape, researchers usually combine magnetic-based indicators with electron delocalization-based indices to quantify the aromatic character of all-metal clusters. While, despite their relevance, resonance energies are rarely computed because of inherent difficulties in their definition. Supplementing these measures with an analysis of existing electron counting rules provides invaluable qualitative insights, even if these rules do not offer a quantitative metric.

The journey since the discovery of the first all-metal aromatic cluster, Al_4^{2-}, clearly demonstrates how this concept has expanded across the periodic table. This significant progress is not just an academic curiosity; it directly challenges and broadens our foundational understanding of many aspects of the aromaticity concept. As the relevance of aromaticity continues to grow in various fields, it is highly probable that we will see further advancements in connecting the existing rules and formulating new ones in the years ahead. This ongoing evolution will move us closer to a unified theory of aromaticity, which hopefully will provide connections among apparently unrelated aromatic systems.

Author contributions

M. S.: conceptualization, writing – original draft, writing – review & editing; A. M.-C.: conceptualization, writing – original draft, writing – review & editing.

Conflicts of interest

There are no conflicts to declare.

This journal is © The Royal Society of Chemistry 2025

Open Access Article. Published on 06 2025. Downloaded on 01.02.26 18:10:06.
This article is licensed under a Creative Commons Attribution-NonCommercial 3.0 Unported Licence.

Data availability

No primary research results, software or code have been included and no new data were generated or analysed as part of this review.

Acknowledgements

M. S. is grateful for financial support from the Agencia Española de Investigación (MCIN/AEI/10.13039/501100011033) for the project PID2023-147424NB-I00 and from the Generalitat de Catalunya for the project 2021SGR623 and ICREA Academia Prize 2024. A. M.-C. is grateful for FONDECYT ANID Regular 1221676.

Notes and references

1 M. Faraday, *Philos. Trans. R. Soc. London*, 1825, **115**, 440–466.
2 A. Ciesielski, T. M. Krygowski, M. K. Cyrański, M. A. Dobrowolski and A. T. Balaban, *J. Chem. Inf. Model.*, 2009, **49**, 369–376.
3 A. F. Pozharskii, *Chem. Heterocycl. Compd.*, 1985, **21**, 717–749.
4 *Structure, Bonding and Reactivity of Heterocyclic Compounds*, ed. F. De Proft and P. Geerlings, Springer Berlin Heidelberg, Berlin, Heidelberg, 2014, vol. 38.
5 A. Artigas and M. Solà, in *Molecular Nanographenes: Synthesis, Properties, and Applications*, ed. N. Martín and C. P. Nuckolls, Wiley-VCH Weinheim, Germany, 2025, pp. 1–30.
6 J. R. Bleeke, *Chem. Rev.*, 2001, **101**, 1205–1228.
7 B. Xu, W. Mao, Z. Lu, Y. Cai, D. Chen and H. Xia, *Nat. Commun.*, 2024, **15**, 4378.
8 A. I. Boldyrev and L.-S. Wang, *Chem. Rev.*, 2005, **105**, 3716–3757.
9 H. Zhai, A. E. Kuznetsov, A. I. Boldyrev and L. Wang, *ChemPhysChem*, 2004, **5**, 1885–1891.
10 D. Y. Zubarev and A. I. Boldyrev, in *Science and Technology of Atomic, Molecular, Condensed Matter & Biological Systems*, ed. P. Jena and A. W. Castleman, Elsevier, Dordrecht, 2010, pp. 219–267.
11 A. E. Kuznetsov, K. A. Birch, A. I. Boldyrev, X. Li, H.-J. Zhai and L.-S. Wang, *Science*, 2003, **300**, 622–625.
12 M. Solà, A. I. Boldyrev, M. K. Cyranski, T. M. Krygowski and G. Merino, *Aromaticity and Antiaromaticity*, Wiley, Chichester, 2023, pp. 35–54.
13 X. Li, A. E. Kuznetsov, H.-F. Zhang, A. I. Boldyrev and L.-S. Wang, *Science*, 2001, **291**, 859–861.
14 J. M. Mercero, I. Infante and J. M. Ugalde, in *Aromaticity and Metal Clusters*, ed. P. K. Chattaraj, CRC Press, Boca Raton, 2011, pp. 345–360.
15 E. Hückel, *Z. Phys.*, 1931, **70**, 204–286.
16 E. Hückel, *Z. Phys.*, 1931, **72**, 310–337.
17 E. Hückel, *Z. Phys.*, 1932, **76**, 628–648.
18 E. Hückel, *Z. Elektrochem. Angew. Phys. Chem.*, 1937, **43**, 752–788.
19 R. W. A. Havenith and J. H. van Lenthe, *Chem. Phys. Lett.*, 2004, **385**, 198–201.
20 R. W. A. Havenith, F. De Proft, P. W. Fowler and P. Geerlings, *Chem. Phys. Lett.*, 2005, **407**, 391–396.
21 A. I. Boldyrev and A. E. Kuznetsov, *Inorg. Chem.*, 2002, **41**, 532–537.
22 P. W. Fowler, R. W. A. Havenith and E. Steiner, *Chem. Phys. Lett.*, 2002, **359**, 530–536.
23 R. W. A. Havenith and P. W. Fowler, *Phys. Chem. Chem. Phys.*, 2006, **8**, 3383.
24 R. Islas, T. Heine and G. Merino, *J. Chem. Theory Comput.*, 2007, **3**, 775–781.
25 J. Jusélius, M. Straka and D. Sundholm, *J. Phys. Chem. A*, 2001, **105**, 9939–9944.
26 Y.-C. Lin, J. Jusélius, D. Sundholm and J. Gauss, *J. Chem. Phys.*, 2005, **122**, 214308.
27 F. Feixas, E. Matito, M. Duran, J. Poater and M. Solà, *Theor. Chem. Acc.*, 2011, **128**, 419–431.
28 M. Solà, F. Feixas, J. O. C. Jiménez-Halla, E. Matito and J. Poater, *Symmetry*, 2010, **2**, 1156–1179.
29 C. A. Tsipis, *Coord. Chem. Rev.*, 2005, **249**, 2740–2762.
30 F. Feixas, E. Matito, J. Poater and M. Solà, *Wiley Interdiscip. Rev.: Comput. Mol. Sci.*, 2013, **3**, 105–122.
31 J. M. Mercero, A. I. Boldyrev, G. Merino and J. M. Ugalde, *Chem. Soc. Rev.*, 2015, **44**, 6519–6534.
32 D. Y. Zubarev, B. B. Averkiev, H.-J. Zhai, L.-S. Wang and A. I. Boldyrev, *Phys. Chem. Chem. Phys.*, 2008, **10**, 257–267.
33 R. Hoffmann, *Am. Sci.*, 2015, **103**, 18–22.
34 J. Aihara, *Bull. Chem. Soc. Jpn.*, 1978, **51**, 1788–1792.
35 R. D. Bach, G. J. Wolber and H. B. Schlegel, *J. Am. Chem. Soc.*, 1985, **107**, 2837–2841.
36 M. J. S. Dewar, *Angew. Chem., Int. Ed. Engl.*, 1971, **10**, 761–776.
37 K. N. Houk, J. Gonzalez and Y. Li, *Acc. Chem. Res.*, 1995, **28**, 81–90.
38 H. Jiao and P. von R. Schleyer, *J. Phys. Org. Chem.*, 1998, **11**, 655–662.
39 M. Mandado, M. J. González-Moa and R. A. Mosquera, *ChemPhysChem*, 2007, **8**, 696–702.
40 P. von R. Schleyer, J. I. Wu, F. P. Cossío and I. Fernández, *Chem. Soc. Rev.*, 2014, **43**, 4909–4921.
41 N. C. Baird, *J. Am. Chem. Soc.*, 1972, **94**, 4941–4948.
42 H. Ottosson, *Nat. Chem.*, 2012, **4**, 969–971.
43 L. J. Karas and J. I. Wu, *Nat. Chem.*, 2022, **14**, 723–725.
44 Z. Chen, C. S. Wannere, C. Corminboeuf, R. Puchta and P. von R. Schleyer, *Chem. Rev.*, 2005, **105**, 3842–3888.
45 P. Bultinck, R. Ponec and S. Van Damme, *J. Phys. Org. Chem.*, 2005, **18**, 706–718.
46 E. Matito, M. Duran and M. Solà, *J. Chem. Phys.*, 2005, **122**, 014109.
47 E. Matito, B. Silvi, M. Duran and M. Solà, *J. Chem. Phys.*, 2006, **125**, 059901.
48 C. F. Matta, *J. Comput. Chem.*, 2003, **24**, 453–463.
49 C. F. Matta and J. Hernández-Trujillo, *J. Phys. Chem. A*, 2003, **107**, 7496–7504.
50 J. Kruszewski and T. M. Krygowski, *Tetrahedron Lett.*, 1972, **13**, 3839–3842.
51 T. M. Krygowski, *J. Chem. Inf. Comput. Sci.*, 1993, **33**, 70–78.
52 C.-G. Zhan, F. Zheng and D. A. Dixon, *J. Am. Chem. Soc.*, 2002, **124**, 14795–14803.
53 M. K. Cyrański, *Chem. Rev.*, 2005, **105**, 3773–3811.
54 H. Fliegl, S. Taubert, O. Lehtonen and D. Sundholm, *Phys. Chem. Chem. Phys.*, 2011, **13**, 20500–20518.
55 P. Lazzeretti, *Theor. Chem. Acc.*, 2012, **131**, 1222.
56 A. Soncini, P. Lazzeretti and R. Zanasi, *Chem. Phys. Lett.*, 2006, **421**, 21–26.
57 R. Herges and D. Geuenich, *J. Phys. Chem. A*, 2001, **105**, 3214–3220.
58 D. Geuenich, K. Hess, F. Köhler and R. Herges, *Chem. Rev.*, 2005, **105**, 3758–3772.
59 P. von R. Schleyer, C. Maerker, A. Dransfeld, H. Jiao and N. J. R. van E. Hommes, *J. Am. Chem. Soc.*, 1996, **118**, 6317–6318.
60 J. O. C. Jiménez-Halla, E. Matito, J. Robles and M. Solà, *J. Organomet. Chem.*, 2006, **691**, 4359–4366.
61 A. Stanger, *J. Org. Chem.*, 2006, **71**, 883–893.
62 R. Gershoni-Poranne and A. Stanger, *Chem. – Eur. J.*, 2014, **20**, 5673–5688.
63 T. Heine, P. V. R. Schleyer, C. Corminboeuf, G. Seifert, R. Reviakine and J. Weber, *J. Phys. Chem. A*, 2003, (107), 6470–6475.
64 S. Klod, A. Koch and E. Kleinpeter, *J. Chem. Soc., Perkin Trans. 2*, 2002, 1506–1509.
65 B. J. Lampkin, P. B. Karadakov and B. VanVeller, *Angew. Chem., Int. Ed.*, 2020, **59**, 19275–19281.
66 A. Artigas, D. Hagebaum-Reignier, Y. Carissan and Y. Coquerel, *Chem. Sci.*, 2021, **12**, 13092–13100.
67 C. Foroutan-Nejad, *Theor. Chem. Acc.*, 2015, **134**, 8.
68 M. Orozco-Ic, L. Soriano-Agueda, D. Sundholm, E. Matito and G. Merino, *Chem. Sci.*, 2024, **15**, 12906–12921.
69 J. Poater, M. Duran, M. Solà and B. Silvi, *Chem. Rev.*, 2005, **105**, 3911–3947.
70 F. Feixas, E. Matito, J. Poater and M. Solà, *Chem. Soc. Rev.*, 2015, **44**, 6434–6451.
71 M. Giambiagi, M. Segre de Giambiagi, C. D. dos Santos Silva and A. Paiva de Figueiredo, *Phys. Chem. Chem. Phys.*, 2000, **2**, 3381–3392.
72 R. F. W. Bader, A. Streitwieser, A. Neuhaus, K. E. Laidig and P. Speers, *J. Am. Chem. Soc.*, 1996, **118**, 4959–4965.
73 X. Fradera, M. A. Austen and R. F. W. Bader, *J. Phys. Chem. A*, 1999, **103**, 304–314.
74 X. Fradera, J. Poater, S. Simon, M. Duran and M. Solà, *Theor. Chem. Acc.*, 2002, **108**, 214–224.

Open Access Article. Published on 06 2025. Downloaded on 01.02.26 18:10:06. This article is licensed under a Creative Commons Attribution-NonCommercial 3.0 Unported Licence.

75 A. D. Becke and K. E. Edgecombe, *J. Chem. Phys.*, 1990, **92**, 5397–5403.
76 J. C. Santos, W. Tiznado, R. Contreras and P. Fuentealba, *J. Chem. Phys.*, 2004, **120**, 1670–1673.
77 J. C. Santos, J. Andres, A. Aizman and P. Fuentealba, *J. Chem. Theory Comput.*, 2005, **1**, 83–86.
78 H. L. Schmider and A. D. Becke, *J. Mol. Struct.:THEOCHEM*, 2000, **527**, 51–61.
79 V. Tsirelson and A. Stash, *Acta Crystallogr., Sect. B: Struct. Sci.*, 2002, **58**, 780–785.
80 H. Jacobsen, *Can. J. Chem.*, 2008, **86**, 695–702.
81 Z. Liu, T. Lu, S. Hua and Y. Yu, *J. Phys. Chem. C*, 2019, **123**, 18593–18599.
82 D. W. Szczepanik, *Comput. Theor. Chem.*, 2016, **1080**, 33–37.
83 D. W. Szczepanik, M. Solà, T. M. Krygowski, H. Szatylowicz, M. Andrzejak, B. Pawełek, J. Dominikowska, M. Kukułka and K. Dyduch, *Phys. Chem. Chem. Phys.*, 2018, **20**, 13430–13436.
84 H. C. Longuet-Higgins and L. Salem, *Philos. Trans. R. Soc., A*, 1959, **251**, 172–185.
85 N. C. Baird and R. M. West, *J. Am. Chem. Soc.*, 1971, **93**, 4427–4432.
86 A. Hirsch, Z. Chen and H. Jiao, *Angew. Chem., Int. Ed.*, 2000, **39**, 3915–3917.
87 D. Y. Zubarev and A. I. Boldyrev, *Phys. Chem. Chem. Phys.*, 2008, **10**, 5207–5217.
88 P. K. Chattaraj, *Aromaticity and Metal Clusters*, CRC Press, Boca Raton, 2010.
89 X. Wang, Z.-C. Han, W. Wei, H. Hu, P. Li, P. Sun, X. Liu, Z. Lv, F. Wang, Y. Cao, Z. Guo, J. Li and J. Zhao, *Chem. Sci.*, 2022, **13**, 7269–7275.
90 J. Wang, C. Luo, C. Shan, Q. You, J. Lu, S. Elf, Y. Zhou, Y. Wen, J. L. Vinkenborg, J. Fan, H. Kang, R. Lin, D. Han, Y. Xie, J. Karpus, S. Chen, S. Ouyang, C. Luan, N. Zhang, H. Ding, M. Merkx, H. Liu, J. Chen, H. Jiang and C. He, *Nat. Chem.*, 2015, **7**, 968–979.
91 J. O. C. Jiménez-Halla, E. Matito, L. Blancafort, J. Robles and M. Solà, *J. Comput. Chem.*, 2009, **30**, 2764–2776.
92 J. O. C. Jiménez-Halla, E. Matito, L. Blancafort, J. Robles and M. Solà, *J. Comput. Chem.*, 2011, **32**, 372–373.
93 S. Giri, D. R. Roy, S. Duley, A. Chakraborty, R. Parthasarathi, M. Elango, R. Vijayaraj, V. Subramanian, R. Islas, G. Merino and P. K. Chattaraj, *J. Comput. Chem.*, 2010, **31**, 1815–1821.
94 L. Yong, S. D. Wu and X. X. Chi, *Int. J. Quantum Chem.*, 2007, **107**, 722–728.
95 X. X. Chi and Y. Liu, *Int. J. Quantum Chem.*, 2007, **107**, 1886–1896.
96 X.-W. Li, W. T. Pennington and G. H. Robinson, *J. Am. Chem. Soc.*, 1995, **117**, 7578–7579.
97 Y. Xie, P. R. Schreiner, H. F. Schaefer, X.-W. Li and G. H. Robinson, *J. Am. Chem. Soc.*, 1996, **118**, 10635–10639.
98 R. J. Wright, M. Brynda and P. P. Power, *Angew. Chem., Int. Ed.*, 2006, **45**, 5953–5956.
99 J. Jin, G. Wang, M. Zhou, D. M. Andrada, M. Hermann and G. Frenking, *Angew. Chem., Int. Ed.*, 2016, **55**, 2078–2082.
100 M. Wang and Y. Wang, *Molecules*, 2024, **29**, 763.
101 F. Feixas, J. O. C. Jiménez-Halla, E. Matito, J. Poater and M. Solà, *J. Chem. Theory Comput.*, 2010, **6**, 1118–1130.
102 Y. Haas and S. Zilberg, *J. Am. Chem. Soc.*, 1995, **117**, 5387–5388.
103 P. C. Hiberty, D. Danovich, A. Shurki and S. Shaik, *J. Am. Chem. Soc.*, 1995, **117**, 7760–7768.
104 S. C. A. H. Pierrefixe and F. M. Bickelhaupt, *Chem. – Eur. J.*, 2007, **13**, 6321–6328.
105 J. Poater, F. Feixas, F. M. Bickelhaupt and M. Solà, *Phys. Chem. Chem. Phys.*, 2011, **13**, 20673–20681.
106 R. Islas, J. Poater, E. Matito and M. Solà, *Phys. Chem. Chem. Phys.*, 2012, **14**, 14850–14859.
107 E. Díaz-Cervantes, J. Poater, J. Robles, M. Swart and M. Solà, *J. Phys. Chem. A*, 2013, **117**, 10462–10469.
108 D. Chen, D. W. Szczepanik, J. Zhu and M. Solà, *Chem. Commun.*, 2020, **56**, 12522–12525.
109 H. Zhang, L. Leyva-Parra, L. Cui, W. Tiznado and Z. Cui, *J. Chem. Phys.*, 2025, **162**, 164308.
110 P. Chen, Y. Li, J. Ma, J. Zhu, J. Xie, M. Solà, C. Zhu and Q. Zhu, *J. Am. Chem. Soc.*, 2025, **147**, 14769–14776.
111 A. W. Castleman and S. N. Khanna, *J. Phys. Chem. C*, 2009, **113**, 2664–2675.
112 S. N. Khanna, A. C. Reber, D. Bista, T. Sengupta and R. Lambert, *J. Chem. Phys.*, 2021, **155**, 120901.
113 H. Häkkinen, *Chem. Soc. Rev.*, 2008, **37**, 1847–1859.
114 Z. Chen, S. Neukermans, X. Wang, E. Janssens, Z. Zhou, R. E. Silverans, R. B. King, P. von R. Schleyer and P. Lievens, *J. Am. Chem. Soc.*, 2006, **128**, 12829–12834.
115 H. W. Kroto, J. R. Heath, S. C. O'Brien, R. F. Curl and R. E. Smalley, *et al.*, *Nature*, 1985, **318**, 162–163.
116 M. Mulet-Gas, L. Abella, P. W. Dunk, A. Rodríguez-Fortea, H. W. Kroto and J. M. Poblet, *Chem. Sci.*, 2015, **6**, 675–686.
117 E. Sheka, *Fullerenes: Nanochemistry, Nanomagnetism, Nanomedicine, Nanophotonics*, CRC Press, Boca Raton, 2011.
118 E. A. Doud, A. Voevodin, T. J. Hochuli, A. M. Champsaur, C. Nuckolls and X. Roy, *Nat. Rev. Mater.*, 2020, **5**, 371–387.
119 T. A. Barendt, M. L. Ball, Q. Xu, B. Zhang, B. Fowler, A. Schattman, V. C. Ritter, M. L. Steigerwald and C. Nuckolls, *Chem. – Eur. J.*, 2020, **26**, 3744–3748.
120 K. M. Kadish and R. S. Ruoff, *Fullerenes: Chemistry, Physics, and Technology*, John Wiley & Sons Ltd, New York, NY, 2000.
121 P. Anilkumar, F. Lu, L. Cao, P. G. Luo, J.-H. Liu, S. Sahu, K. N. Tackett II, Y. Wang and Y.-P. Sun, *Curr. Med. Chem.*, 2011, **18**, 2045–2059.
122 K. Kurotobi and Y. Murata, *Science*, 2011, **333**, 613–616.
123 A. Rodríguez-Fortea, N. Alegret and J. M. Poblet, *Comprehensive Inorganic Chemistry II*, Elsevier, Dordrecht, 2013, pp. 907–924.
124 S. Osuna, M. Swart and M. Solà, *Phys. Chem. Chem. Phys.*, 2011, **13**, 3585–3603.
125 V. Elser and R. C. Haddon, *Nature*, 1987, **325**, 792–794.
126 M. Bühl and A. Hirsch, *Chem. Rev.*, 2001, **101**, 1153–1184.
127 J. Aihara, *J. Mol. Struct.*, 1994, **311**, 1–8.
128 Z. Chen, J. I. Wu, C. Corminboeuf, J. Bohmann, X. Lu, A. Hirsch and P. von R. Schleyer, *Phys. Chem. Chem. Phys.*, 2012, **14**, 14886–14891.
129 M. Gaboardi, S. Duyker, C. Milanese, G. Magnani, V. K. Peterson, D. Pontiroli, N. Sharma and M. Riccò, *J. Phys. Chem. C*, 2015, **119**, 19715–19721.
130 A. Ahmed, A. W. Thornton, K. Konstas, S. K. Kannam, R. Babarao, B. D. Todd, A. J. Hill and M. R. Hill, *Langmuir*, 2013, **29**, 15689–15697.
131 J. A. Teprovich, M. S. Wellons, R. Lascola, S.-J. Hwang, P. A. Ward, R. N. Compton and R. Zidan, *Nano Lett.*, 2012, **12**, 582–589.
132 M. Garcia-Borràs, S. Osuna, J. M. Luis, M. Swart and M. Solà, *Chem. Soc. Rev.*, 2014, **43**, 5089–5105.
133 M. P. Johansson, D. Sundholm and J. Vaara, *Angew. Chem., Int. Ed.*, 2004, **43**, 2678–2681.
134 A. F. Jalbout, F. F. Contreras-Torres, L. A. Pérez and I. L. Garzón, *J. Phys. Chem. A*, 2008, **112**, 353–357.
135 M. Ji, X. Gu, X. Li, X. Gong, J. Li and L. Wang, *Angew. Chem., Int. Ed.*, 2005, **44**, 7119–7123.
136 A. J. Karttunen, M. Linnolahti, T. A. Pakkanen and P. Pyykkö, *Chem. Commun.*, 2008, 465–467.
137 W. Ekardt, *Phys. Rev. B: Condens. Matter Mater. Phys.*, 1984, **29**, 1558–1564.
138 M. L. Cohen, M. Y. Chou, W. D. Knight and W. A. De Heer, *J. Phys. Chem.*, 1987, **91**, 3141–3149.
139 W. A. de Heer, *Rev. Mod. Phys.*, 1993, **65**, 611–676.
140 W. D. Knight, K. Clemenger, W. A. de Heer, W. A. Saunders, M. Y. Chou and M. L. Cohen, *Phys. Rev. Lett.*, 1984, **52**, 2141–2143.
141 V. Cerowski, B. K. Rao, S. N. Khanna, P. Jena, S. Ishii, K. Ohno and Y. Kawazoe, *J. Chem. Phys.*, 2005, **123**, 074329.
142 J. Poater and M. Solà, *Chem. Commun.*, 2019, **55**, 5559–5562.
143 O. El Bakouri, V. Postils, M. Garcia-Borràs, M. Duran, J. M. Luis, S. Calvello, A. Soncini, E. Matito, F. Feixas and M. Solà, *Chem. – Eur. J.*, 2018, **24**, 9853–9859.
144 Y.-H. Xu, W.-J. Tian, A. Muñoz-Castro, G. Frenking and Z.-M. Sun, *Science*, 2023, **382**, 840–843.
145 A. Muñoz-Castro, *Phys. Chem. Chem. Phys.*, 2017, **19**, 12633–12636.
146 N. D. Charistos and A. Muñoz-Castro, *J. Phys. Chem. C*, 2018, **122**, 9688–9698.
147 A. G. Papadopoulos, N. D. Charistos and A. Muñoz-Castro, *ChemPhysChem*, 2017, **18**, 1499–1502.
148 P. von R. Schleyer and H. Jiao, *Pure Appl. Chem.*, 1996, **68**, 209–218.
149 S. Mondal and P. K. Chattaraj, *Energies*, 2023, **16**, 2833.
150 O. El Bakouri, M. Duran, J. Poater, F. Feixas and M. Solà, *Phys. Chem. Chem. Phys.*, 2016, **18**, 11700–11706.
151 R. B. King, T. Heine, C. Corminboeuf and P. von R. Schleyer, *J. Am. Chem. Soc.*, 2004, **126**, 430–431.
152 S. Srinivas and J. Jellinek, *J. Chem. Phys.*, 2004, **121**, 7243–7252.

 This journal is © The Royal Society of Chemistry 2025

Open Access Article. Published on 06 2025. Downloaded on 01.02.26 18:10:06.
This article is licensed under a Creative Commons Attribution-NonCommercial 3.0 Unported Licence.

153 A. E. Kuznetsov, A. I. Boldyrev, H. J. Zhai, X. Li and L. S. Wang, *J. Am. Chem. Soc.*, 2002, **124**, 11791–11801.
154 O. El Bakouri, M. Solà and J. Poater, *Phys. Chem. Chem. Phys.*, 2016, **18**, 21102–21110.
155 O. El Bakouri, M. Solà and J. Poater, *Phys. Chem. Chem. Phys.*, 2018, **20**, 3845–3846.
156 W. L. Cao, C. Gatti, P. J. MacDougall and R. F. W. Bader, *Chem. Phys. Lett.*, 1987, **141**, 380–385.
157 V. Postils, M. Garcia-Borràs, M. Solà, J. M. Luis and E. Matito, *Chem. Commun.*, 2015, **51**, 4865–4868.
158 T. F. Fässler, *Zintl Ions*, Springer Berlin Heidelberg, Berlin, Heidelberg, 2011, vol. 140.
159 C. Liu and Z.-M. Sun, *Coord. Chem. Rev.*, 2019, **382**, 32–56.
160 S. Scharfe, F. Kraus, S. Stegmaier, A. Schier and T. F. Fässler, *Angew. Chem., Int. Ed.*, 2011, **50**, 3630–3670.
161 S. M. Kauzlarich, *Chem. Mater.*, 2023, **35**, 7355–7362.
162 S. Fang, J. Li, K. Zou, H. Shuai, L. Xu, W. Deng, G. Zou, H. Hou and X. Ji, *Chem. Eng. J.*, 2022, **433**, 133841.
163 R. J. Wilson, B. Weinert and S. Dehnen, *Dalton Trans.*, 2018, **47**, 14861–14869.
164 F. Pan, L. Guggolz and S. Dehnen, *CCS Chem.*, 2022, **4**, 809–824.
165 J. Zhou, S. Giri and P. Jena, *Phys. Chem. Chem. Phys.*, 2014, **16**, 20241–20247.
166 R. Parida, G. N. Reddy, A. Ganguly, G. Roymahapatra, A. Chakraborty and S. Giri, *Chem. Commun.*, 2018, **54**, 3903–3906.
167 C. Liu, I. A. Popov, Z. Chen, A. I. Boldyrev and Z.-M. Sun, *Chem. – Eur. J.*, 2018, **24**, 14583–14597.
168 J. E. McGrady, F. Weigend and S. Dehnen, *Chem. Soc. Rev.*, 2022, **51**, 628–649.
169 M. Raupach, S. Dehnen and R. Tonner, *J. Comput. Chem.*, 2014, **35**, 1045–1057.
170 K. Wade, *J. Chem. Soc. D*, 1971, 792–793.
171 D. M. P. Mingos, *Nat. Phys. Sci.*, 1972, **236**, 99–102.
172 K. Wade, *Adv. Inorg. Chem. Radiochem.*, 1976, **18**, 1–66.
173 C. Liu, X. Jin, L.-J. Li, J. Xu, J. E. McGrady and Z.-M. Sun, *Chem. Sci.*, 2019, **10**, 4394–4401.
174 A. Spiekermann, S. D. Hoffmann and T. F. Fässler, *Angew. Chem., Int. Ed.*, 2006, **45**, 3459–3462.
175 A. Li, Y. Wang, D. O. Downing, F. Chen, P. Zavalij, A. Muñoz-Castro and B. W. Eichhorn, *Chem. – Eur. J.*, 2020, **26**, 5824–5833.
176 A. Grubisic, H. Wang, X. Li, Y.-J. Ko, F. S. Kocak, M. R. Pederson, K. H. Bowen and B. W. Eichhorn, *Proc. Natl. Acad. Sci. U. S. A.*, 2011, **108**, 14757–14762.
177 E. N. Esenturk, J. Fettinger and B. Eichhorn, *Chem. Commun.*, 2005, 247–249.
178 Z. Chen, H. Jiao, A. Hirsch and W. Thiel, *Mol. Modell. Annu.*, 2001, **7**, 161–163.
179 A. Hirsch, Z. Chen and H. Jiao, *Angew. Chem., Int. Ed.*, 2001, **40**, 2834–2838.
180 L.-F. Cui, X. Huang, L.-M. Wang, D. Y. Zubarev, A. I. Boldyrev, J. Li and L.-S. Wang, *J. Am. Chem. Soc.*, 2006, **128**, 8390–8391.
181 L.-F. Cui, X. Huang, L.-M. Wang, J. Li and L.-S. Wang, *J. Phys. Chem. A*, 2006, **110**, 10169–10172.
182 L. Cui, X. Huang, L. Wang, J. Li and L. Wang, *Angew. Chem., Int. Ed.*, 2007, **46**, 742–745.
183 A. C. Castro, E. Osorio, J. O. C. Jiménez-Halla, E. Matito, W. Tiznado and G. Merino, *J. Chem. Theory Comput.*, 2010, **6**, 2701–2705.
184 L.-J. Li, F.-X. Pan, F.-Y. Li, Z.-F. Chen and Z.-M. Sun, *Inorg. Chem. Front.*, 2017, **4**, 1393–1396.
185 R. J. Wilson, N. Lichtenberger, B. Weinert and S. Dehnen, *Chem. Rev.*, 2019, **119**, 8506–8554.
186 B. Huo, X.-L. Guan, C. Yuan and Y.-B. Wu, *Inorg. Chem.*, 2025, **64**, 3000–3007.
187 P. L. Rodríguez-Kessler and A. Muñoz-Castro, *Phys. Chem. Chem. Phys.*, 2024, **26**, 8419–8425.
188 A. S. Pozdeev, A. I. Boldyrev and Y. Rao, *Polyhedron*, 2023, **243**, 116572.
189 Y.-H. Xu, X. Yang, Y.-N. Yang, L. Zhao, G. Frenking and Z.-M. Sun, *Nat. Chem.*, 2025, **17**, 556–563.
190 J. Rienmüller, B. Peerless, S. Paul, F. Bruder, W. Wernsdorfer, F. Weigend and S. Dehnen, *Nat. Chem.*, 2025, **17**, 547–555.
191 A. R. Eulenstein, Y. J. Franzke, N. Lichtenberger, R. J. Wilson, H. L. Deubner, F. Kraus, R. Clérac, F. Weigend and S. Dehnen, *Nat. Chem.*, 2021, **13**, 149–155.
192 B. Peerless, A. Schmidt, Y. J. Franzke and S. Dehnen, *Nat. Chem.*, 2023, **15**, 347–356.
193 I. Todorov and S. C. Sevov, *Inorg. Chem.*, 2005, **44**, 5361–5369.
194 I. Todorov and S. C. Sevov, *Inorg. Chem.*, 2004, **43**, 6490–6494.
195 O. Kysliak, S. H. F. Schreiner, N. Grabicki, P. Liebing, F. Weigend, O. Dumele and R. Kretschmer, *Angew. Chem., Int. Ed.*, 2022, **61**, e202206963.
196 L. Alvarez-Thon and N. Inostroza-Pino, *J. Comput. Chem.*, 2018, **39**, 862–868.
197 C. Xu, T. Wang, C. Wang, X. Dong, H. Zheng, Y. Zhao, L. Pan, J. Yang, W. Zhang, G. Wu, H. Xie, G. Li, J. Li, L. Jiang, X. Yang and L. Wang, *Angew. Chem., Int. Ed.*, 2025, **64**, e202419089.
198 H. G. von Schnering, U. Bolle, J. Curda, K. Peters, W. Carrillo-Cabrera, M. Somer, M. Schultheiss and U. Wedig, *Angew. Chem., Int. Ed. Engl.*, 1996, **35**, 984–986.
199 R. Yadav, A. Maiti, M. Schorpp, J. Graf, F. Weigend and L. Greb, *Nat. Chem.*, 2024, **16**, 1523–1530.
200 G. Merino, M. Solà, I. Fernández, C. Foroutan-Nejad, P. Lazzeretti, G. Frenking, H. L. Anderson, D. Sundholm, F. P. Cossío, M. A. Petrukhina, J. Wu, J. I. Wu and A. Restrepo, *Chem. Sci.*, 2023, **14**, 5569–5576.
201 S. Stegmaier and T. F. Fässler, *J. Am. Chem. Soc.*, 2011, **133**, 19758–19768.
202 M. Kulichenko, N. Fedik, A. Boldyrev and A. Muñoz-Castro, *Chem. – Eur. J.*, 2020, **26**, 2263–2268.
203 A. Muñoz-Castro and R. B. King, *Inorg. Chem.*, 2017, **56**, 15251–15258.
204 P. L. Rodríguez-Kessler, N. D. Charistos, R. B. King and A. Muñoz-Castro, *Phys. Chem. Chem. Phys.*, 2020, **22**, 14268–14275.
205 A. Miralrio, A. Muñoz-Castro, R. B. King and L. E. Sansores, *J. Phys. Chem. C*, 2019, **123**, 1429–1443.
206 A. Muñoz-Castro and R. B. B. King, *Phys. Chem. Chem. Phys.*, 2020, **22**, 23920–23928.
207 J. M. Goicoechea and S. C. Sevov, *J. Am. Chem. Soc.*, 2005, **127**, 7676–7677.
208 Z.-M. Sun, H. Xiao, J. Li and L.-S. Wang, *J. Am. Chem. Soc.*, 2007, **129**, 9560–9561.
209 P. L. Rodríguez-Kessler and A. Muñoz-Castro, *Nanoscale*, 2024, **16**, 5829–5835.
210 Y.-S. Huang, H.-L. Xu, W.-J. Tian, Z.-S. Li, S. Escayola, M. Solà, A. Muñoz-Castro and Z.-M. Sun, *J. Am. Chem. Soc.*, 2025, **147**, 9407–9414.
211 D. W. Szczepanik, M. Andrzejak, J. Dominikowska, B. Pawełek, T. M. Krygowski, H. Szatylowicz and M. Solà, *Phys. Chem. Chem. Phys.*, 2017, **19**, 28970–28981.
212 D. W. Szczepanik, M. Andrzejak, K. Dyduch, E. Żak, M. Makowski, G. Mazur and J. Mrozek, *Phys. Chem. Chem. Phys.*, 2014, **16**, 20514–20523.
213 D. W. Szczepanik, E. Żak, K. Dyduch and J. Mrozek, *Chem. Phys. Lett.*, 2014, **593**, 154–159.
214 D. Sundholm, H. Fliegl and R. J. F. Berger, *Wiley Interdiscip. Rev.: Comput. Mol. Sci.*, 2016, **6**, 639–678.
215 T. Heine, C. Corminboeuf and G. Seifert, *Chem. Rev.*, 2005, **105**, 3889–3910.
216 G. Merino, T. Heine and G. Seifert, *Chem. – Eur. J.*, 2004, **10**, 4367–4371.